Available online at www.sciencedirect.com
SCIENCE DIRECT®
Journal of Solid State Chemistry 177 (2004) 3254–3262
JOURNAL OF SOLID STATE CHEMISTRY
http://elsevier.com/locate/jssc

Isomorphy of structural phase transitions in $LiTaOSiO_4$, $LiTaOGeO_4$ and titanite, $CaTiOSiO_4$

Thomas Malcherek,[a,*] Anne Bosenick,[b] Lado Cemič,[c] Michael Fechtelkord,[d] and Axel Guttzeit[b]

[a] *Mineralogisches Institut, Universität Heidelberg, Im Neuenheimer Feld 236, D-69120 Heidelberg, Germany*
[b] *Institut für Mineralogie, Universität Münster, Corrensstr. 24, D-48149 Münster, Germany*
[c] *Institut für Geowissenschaften, Universität Kiel, Olshausenstr. 40, Kiel, Germany*
[d] *Institut für Geologie, Mineralogie und Geophysik, Ruhr-Universität Bochum, Universitätsstr. 150, D-44780 Bochum, Germany*

Received 22 December 2003; received in revised form 7 April 2004; accepted 17 May 2004

Available online 20 July 2004

Abstract

Structural phase transitions in $LiTaOGeO_4$ (LTGO) and $LiTaOSiO_4$ (LTSO) have been observed using differential scanning calorimetry, X-ray diffraction and ^{7}Li MAS NMR spectroscopy. LTGO transforms from $P2_1/c$ to $C2/c$ space group symmetry at $T_c = 231$ K, while the isomorphic transition occurs at $T_c = 439$ K in LTSO. An analogous phase transition is known to occur in the structurally related mineral titanite, $CaTiOSiO_4$. Spontaneous strain accompanying this phase transition in LTSO is significantly stronger than in titanite. As in titanite non-vanishing strain components are observable for $T_c < T < T_i$, with a similar ratio T_i/T_c. ^{7}Li MAS NMR spectroscopy in combination with computation of the electric field gradient by first principle methods confirms that the tetrahedral Li coordination environment is retained during the phase transitions in LTGO and in LTSO. In LTSO substantial motional narrowing is observed, indicating increased mobility of the Li cation above 400 K. The narrowing of the spinning sidebands is significantly modified immediately above and below the critical temperature.

Keywords: Phase transition; Antiferroelectric; Titanite; Sphene; Order–disorder

1. Introduction

A common structural topology for compounds of generalized stoichiometry $AMOXO_4$ consists of parallel chains of trans-corner linked MO_6 octahedra, coupled via isolated XO_4-tetrahedra. In the titanite structure type each such tetrahedron links 2 consecutive octahedra of one chain to octahedra in 2 neighbouring chains. Cavities in the resulting $[MOXO_4]$ framework are occupied by cations A. This particular structural topology can host unusual displacive ordering phenomena, as exhibited by the mineral titanite, $CaTiOSiO_4$. Its phase transition from the high symmetry SG $C2/c$ to the low symmetry antiferroelectric phase with SG $P2_1/c$ at $T_c = 487$ K involves precursors of correlated Ti-displacements along the octahedral chain direction [1].

In the high-temperature polymorph of titanite (SG $C2/c$) the Ti-cation is nominally located at the centre of the TiO_6-octahedron, while the low temperature form is characterized by the displacement of Ti towards the chain forming corner oxygen, O1 [2]. Such a displacement leads to the formation of alternating short and long M–O bonds in the chain direction. The appearance of such a displacement pattern is accompanied by the formation of super-structure diffraction maxima with indices $h + k = 2n + 1$. Such an ordered arrangement has been determined for the silicate LTSO [3] under ambient conditions, while LTGO was found to be disordered at room temperature [4]. Recently the transition from this disordered polymorph to the ordered form, isostructural with LTSO, has been observed at $T_c = 231$ K [5].

In titanite the transition to the paraphase as a function of temperature occurs in two steps [1,6]. At $T_c = 487$ K long range correlation between the

*Corresponding author. Fax: +49-6221-54-4805.
E-mail address: tmalch@min.uni-heidelberg.de (T. Malcherek).

0022-4596/$ - see front matter © 2004 Elsevier Inc. All rights reserved.
doi:10.1016/j.jssc.2004.05.043

Ti-displacements is lost in two dimensions, while linear correlation of the locally displaced Ti-cations along the octahedral chain direction disappears only above $T_i = 825$ K [7]. The intermediate phase between T_c and T_i is characterized by a non-vanishing shear component of the spontaneous strain [8].

Here, we describe structural phase transitions in $LiTaOSiO_4$ and compare its properties to the previously described structural transitions in $LiTaOGeO_4$ and in titanite.

2. Experimental

LTGO and LTSO were synthesized from pressed mixtures of Li_2CO_3, Ta_2O_5 and GeO_2 or SiO_2 powders at a maximum temperature of 1323 and 1623 K, respectively. Prior decarbonization of the powder mixtures was carried out below 1200 K. The pellets of LTSO were welded into a Pt/Rh5 capsule in order to avoid Li_2O loss during annealing at 1623 K. The phase purity of both materials was checked using X-ray powder diffraction. LTGO contained traces ($\leqslant 0.5$ wt%) of $LiTaO_3$ and GeO_2, while LTSO contained less than 1 wt% $LiTaO_3$.

2.1. Differential scanning calorimetry

Heat capacity measurements between 133 and 923 K were carried out using a power-compensated differential scanning calorimeter (Perkin-Elmer DSC-7). The measurements were performed in two stages for LTSO: (a) low temperature c_p-measurements between 133 and 348 K and (b) high temperature c_p-measurements between 323 and 923 K. Only the low-temperature region was scanned in the case of LTGO. In the low-temperature region, the transition point of cyclohexan at 186.09 K and its melting point at 279.67 K (ITS-90) were used for temperature calibration. The measurements were carried out under a constant flow of dried helium gas, keeping the calorimeter block thermostated at 93 ± 1 K. In the high-temperature range, the temperature was calibrated against the melting point of indium and the phase transition temperature of Li_2SO_4 [9]. The measurements were made under a constant flow of dried nitrogen gas with the calorimeter block thermostated at 276 ± 1 K (LTSO). The temperature calibration was checked by observing the phase transition temperature of KNO_3 and the melting point of Zn within ± 1 K of the values given by McAdie et al. [10] (401.15 and 692.78 K, respectively). A single crystal synthetic corundum [11] was used for c_p-standardisation. The standard and the sample were placed in cylindrical Au-pans, 6 mm in diameter and covered with a Au-lid. The c_p measurements were performed using the step-scanning method as described in [12]. Most measurements were made over temperature intervals of 100 K with a heating rate of 20 K/min. Calculations of the heat capacities from the three runs (blank run, standard- and sample run) were made according to the description of the scanning method in [13]. Corrections for differences in pan weights, up to 0.1 mg, are included in the automated calculation using c_p-polynomials fitted to the known heat capacity data of gold. Resulting heat capacity data are shown in Fig. 1.

2.2. X-ray powder diffraction

In situ X-ray diffraction measurements were carried out using an Anton Paar HTK1200 furnace on a Philips Xpert diffractometer. Monochromatic $CuK\alpha_1$-radiation was utilized. The powder specimen was pressed into an Al_2O_3 sample holder. Diffraction patterns of LTSO were recorded in the range between 16° and 85° 2θ using a proportional counter with 4 s/step counting time and a stepsize of 0.02°. Statistics were improved by the use of a sample spinner. Lattice parameters were determined using the LeBail method as implemented in the GSAS-program [14]. Peak profiles were modeled using a pseudo-voigt profile function (#3) including asymmetry correction for axial divergence [15]. The resulting lattice parameters of LTSO are shown in Fig. 2.

2.3. NMR spectroscopy

High-temperature static ^7Li nuclear magnetic resonance (NMR) spectra of LTSO were obtained at a transmitter frequency of 155.51 MHz using a Bruker

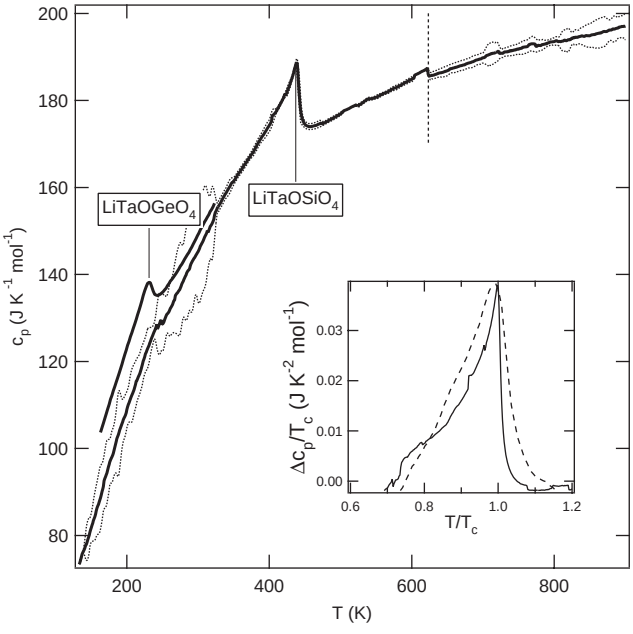

Fig. 1. Heat capacity data for LTGO and LTSO. The dotted lines delineate the esd for LTSO. A vertical dashed line marks the heat capacity jump near 623 K. The inset shows the excess heat capacities of LTSO (solid) and LTGO (dashed) divided by the respective critical temperatures as a function of reduced temperature.

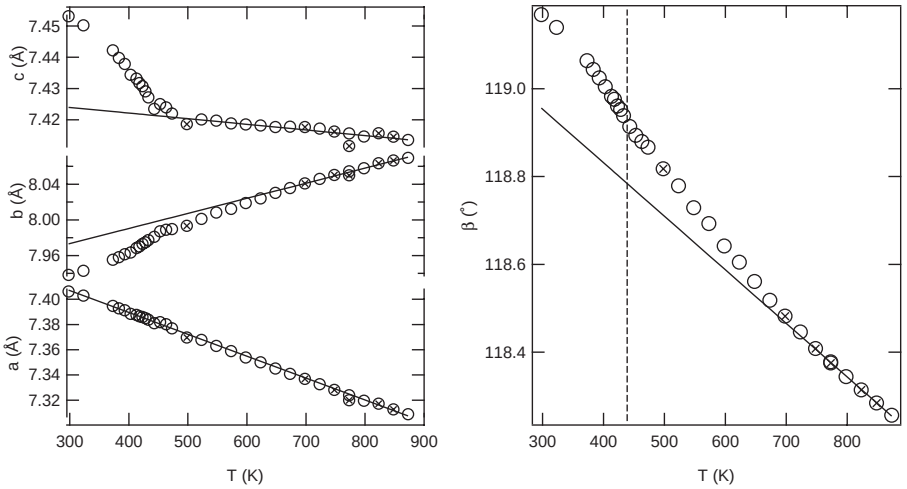

Fig. 2. Lattice parameters of LTSO as a function of temperature. Errors are smaller than the symbol size. Circles denote heating, crossed circles denote cooling. The lines show the assumed linear thermal expansion, extrapolated from the high-temperature data.

ASX 400 NMR spectrometer and a commercial Doty 7 mm HT magic angle spinning (MAS) probehead. This probe design has a closed heating air cycle with a combined bearing/drive air support operating with nitrogen gas. The sample chamber is closed by an evacuated high-grade steel dewar with a copper heat shield. The design enables a constant temperature in the sample chamber and the sample rotor. The temperature gradient along the sample is less than 5 K. Cooling of the probehead surface and the exhaust air is realized by a heat-exchanger and compressed air at ambient temperature. A quadrupolar solid echo $(90_x - \tau - 90_y - \tau - (\mathrm{acq})_x)$ was applied in all static experiments. The 90° pulse length was 6.5 μs. The delay was set to $\tau = 20$ μs. The spectra were accumulated using a spectral width of 500 kHz and a recycle delay of 25 s. A total of 32 scans was accumulated for each static spectrum.

^{7}Li MAS NMR spectra of LTGO between 200 and 290 K and of LTSO between 300 and 500 K were obtained on a high resolution Bruker DSX 500 NMR spectrometer with a magnetic field strength of 11.7 T at 194.38 MHz. Additional spectra of LTGO were obtained using a Bruker CXP 300 NMR spectrometer with a magnetic field strength of 7 T at 116 MHz. One molar aqueous solution of LiCl was used as chemical shift reference at zero ppm for LTGO and for LTSO at ambient temperature, while the high-temperature spectra of LTSO were self referenced. The sideband envelopes of the ^{7}Li spectra were acquired with 6 kHz spinning speed. The simple one-pulse MAS NMR spectra were obtained with 30° pulses of 1.0 μs duration. Between 256 and 1024 free induction decays were accumulated with a recycle delay of 1.0 s. The spectra were acquired with XWINNMR (Bruker) and fitted with DMFIT [16].

2.4. Computation

Values of the electric field gradient (EFG) at the Li-position were calculated from first principles using the full-potential linear augmented plane wave (LAPW) method as implemented in the Wien2k program [17]. The exchange correlation energy was treated in the GGA formalism [18]. Atom coordinates were taken from [3] for LTSO and from [5] for LTGO. The corresponding experimental lattice parameters were used for all calculations. The electronic structure of the $C2/c$ high-temperature phase of LTGO was calculated in a transformed primitive cell setting with 9 atomic positions. Force relaxation of the atomic positions was calculated to less than 0.5 mRy/a.u. in the low symmetry structures. The resulting atomic positions are given in Table 1. These calculations were performed using a plane wave cutoff of $R_{\mathrm{MT}}K_{\max} = 6.5$ and 7 for LTGO and LTSO, respectively. Fifty k-points were sampled in the entire brillouin zone. The default mixed LAPW/APW+lo basis set of Wien2k was used. Values of the calculated EFG component V_{zz} and the asymmetry parameter $\eta = (V_{xx} - V_{yy})/V_{zz}$ are given in Table 2. The corresponding quadrupolar coupling of the Li-atom has been calculated using $C_Q = V_{zz}eQ/h = -9.672 \times 10^{-16} V_{zz}$, where the quadrupolar moment is $Q_{^7\mathrm{Li}} = -0.04$ barn.

3. Results and discussion

3.1. Heat capacity data

As the DSC data show (Fig. 1) both compounds undergo phase transitions accompanied by a strong c_p

Table 1
Structural parameters and residual forces (in mRy/a.u.) by DFT force minimization for LTGO and LTSO in SG symmetry $P2_1/c$ with lattice parameters measured at 173 K and at ambient temperature, respectively

	x	y	z	F_x	F_y	F_z
$LiTaOGeO_4$, $a = 7.584$ Å, $b = 8.085$ Å, $c = 7.508$ Å, $\beta = 119.69°$						
Li	0.74964	0.05715	0.79096	−0.137	−0.047	−0.014
Ta	0.74979	0.75773	0.50414	0.114	−0.063	−0.093
Ge	0.24992	0.61390	0.25833	−0.052	0.066	0.037
O1	0.24882	0.18086	0.24848	−0.056	−0.075	0.071
O21	0.55192	0.26015	0.15360	−0.090	−0.014	0.008
O22	0.94823	0.23944	0.84652	−0.008	−0.155	−0.165
O31	0.74243	0.99018	0.04525	−0.102	−0.033	−0.227
O32	0.75610	0.98871	0.43683	0.277	0.040	−0.208
$LiTaOSiO_4$, $a = 7.4062$ Å, $b = 7.9383$ Å, $c = 7.4532$ Å, $\beta = 119.168°$						
Li	0.75042	0.06647	0.80602	0.036	0.032	0.008
Ta	0.74851	0.75979	0.50617	0.038	−0.266	0.321
Si	0.25035	0.61044	0.25822	−0.119	−0.020	−0.200
O1	0.24924	0.17137	0.24688	0.098	0.124	0.227
O21	0.55785	0.24475	0.14689	0.373	0.198	0.145
O22	0.94408	0.25865	0.85267	−0.333	−0.113	0.240
O31	0.75789	0.99241	0.06610	0.046	−0.184	0.275
O32	0.73675	0.98964	0.41309	0.149	0.025	0.034

Table 2
EFG parameters calculated by first principles and measured by ^{7}Li NMR

Li	Calculated			NMR 300 K	
	V_{zz} (10^{21} V/m^2)	η	C_Q (kHz)	η	C_Q (kHz)
LTGO $P2_1/c$	−0.100	0.18	96.7	0.2	96
LTGO $C2/c$ (4e)	−0.149	0.61	144.3	—	—
LTSO $P2_1/c$	−0.109	0.54	105.4	0.48(2)	95(5)

anomaly. The estimated heat of transition is 810 ± 20 J/mol for LTSO and 320 ± 50 J/mol for LTGO. The baselines were obtained by fitting appropriate polynomial equations to the data outside the reduced temperature interval $0.8 < T/T_c < 1.05$.

Compared to titanite [19], the heat of transition is about 6 times larger in LTSO. The estimated excess heat capacities are shown in Fig. 1, where they have been divided by the corresponding critical temperatures to demonstrate the relative similarity of the thermal properties. In LTSO a second weaker anomaly is observable near 623 K. This anomaly involves a discontinuity of $\Delta c_p = 2$ J/K/mol, indicative of a second-order phase transition.

3.2. X-ray diffraction

During both transitions the diffraction maxima with $h + k = 2n + 1$ disappear. This has been clearly demonstrated for a single crystal of LTGO [5]. Fig. 3a documents the disappearance of the 012 and the $21\bar{2}$-intensities near 440 K in the powder diffraction pattern of LTSO. This confirms a symmetry change $P2_1/c \leftrightarrow C2/c$ in LTSO, analogous to the symmetry change in titanite and in LTGO. Recently, similar results have also been obtained using a single crystal of LTSO [20]. Accordingly the order parameter evolution, $Q(T) = \sqrt{\langle I \rangle / s}$, as a function of temperature is similar to the tricritical mean-field behaviour [1,5,19] of titanite and LTGO (Fig. 3a). The parameter $s = 7.0(5)$ is used to normalize to $Q = 1$ at $T = 0$ K.

3.2.1. Spontaneous strain

With the lattice parameters shown in Fig. 2, the components of the strain tensor e_{ij} are calculated [21], using the extrapolated high-temperature data as reference values to correct for thermal expansion. In order to have the X-direction of the strain tensor oriented parallel to the octahedral chain direction, and thus to facilitate comparison to the data given in [8], the a- and c-lattice dimensions have been interchanged prior to calculation of the tensor-components. The strain data given here for LTSO therefore refer to the A2/a symmetry setting.

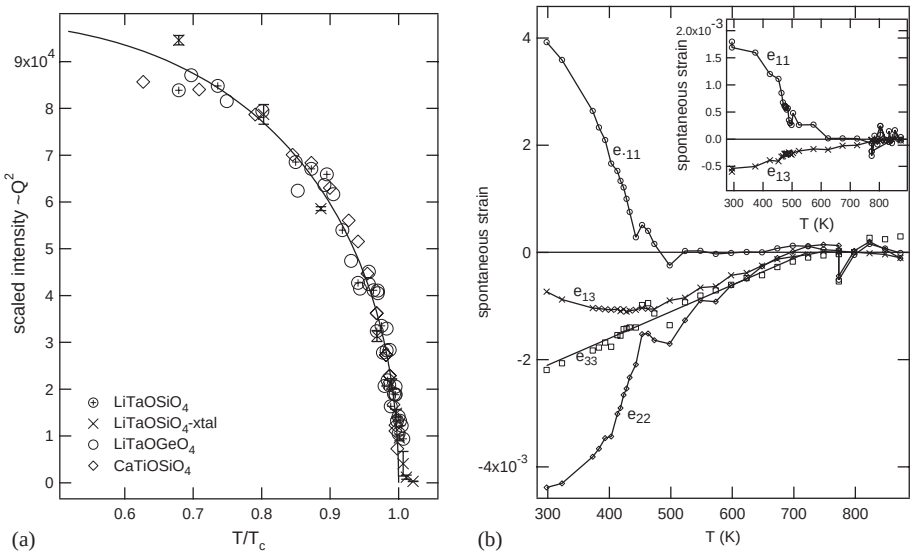

Fig. 3. (a) Scaled superstructure intensities of titanite, LTGO and LTSO as a function of the reduced temperature. The solid curve is the squared solution of the tricritical mean field model. The scaled intensity averages involve the 012- and the $21\bar{2}$-powder reflections of LTSO (powder), the $10\bar{4}$-reflection of a LTSO single crystal [20], the $\bar{3}04$- and $10\bar{4}$-reflections of LTGO [5] and the $10\bar{4}$-reflection of titanite [1]. (b) Strain components of LTSO as a function of the temperature. The inset shows the two significant strain components of titanite for comparison.

While e_{11} increases below T_c, the shear component e_{13} first drops to negative values below 1.7 T/T_c as an almost linear function of temperature, before it increases slightly at temperatures below T_c. The temperature evolution of e_{11} strongly resembles that found in titanite, but the magnitude of the strain is about twice as large in LTSO. The shear component e_{13} is roughly 4 times larger than in titanite. The two remaining strain components e_{22} and e_{33} differ significantly from those of titanite, where e_{22} is absent and e_{33} is very small and negative.

Note that at high temperature the first strain effects become visible at $T_i \gg T_c$. The ratio T_i/T_c is very similar in titanite and in LTSO, as demonstrated by their respective shear components e_{13}. Thus it follows from $T_i/T_c = 825\ \mathrm{K}/487\ \mathrm{K} = 1.69$ in titanite, that $T_i \approx 740$ K in LTSO.

As the c_p data of LTSO in Fig. 1 indicate, a discontinuity occurs near 623 K. This temperature is lower than the estimated temperature T_i and it is therefore not entirely clear whether or not the onset of shear strain can be related to a possible second-order phase transition associated with the c_p-discontinuity. The determination of the spontaneous strain components essentially relies on a linear fit to the high-temperature lattice parameters (Fig. 2). Therefore, the above determination of T_i is certainly more prone to systematic error than the observation of the c_p-jump. Therefore, the coincidence of the onset of shear strain with a second-order phase transition in LTSO is certainly possible. The occurrence of a similar phase transition has been postulated for titanite [7,22].

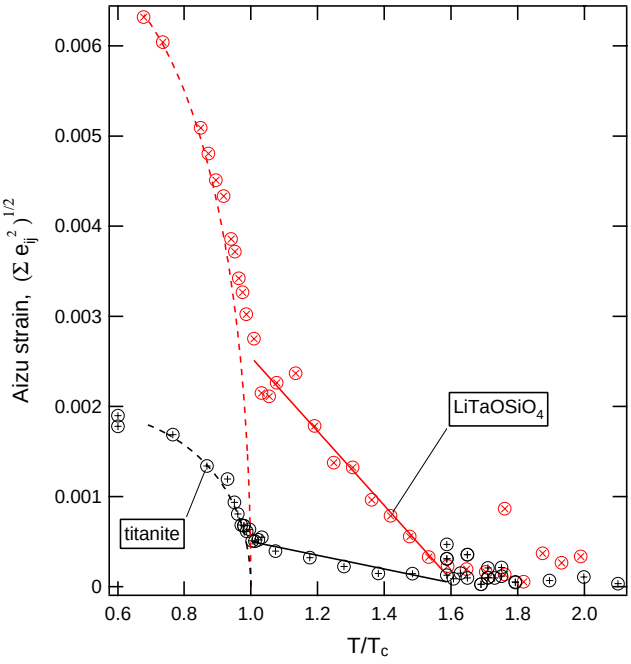

Fig. 4. Scalar strain in LTSO and in titanite as a function of reduced temperature. The dashed lines indicate the scaled temperature evolution of the squared order parameter, calculated using the tricritical mean-field model.

The clearest indication of the parallels between titanite and LTSO in terms of the spontaneous strain data is obtained by comparison of the scalar strain (Aizu strain), defined as $\varepsilon = \sqrt{\sum e_{ij}^2}$ (Fig. 4).

Given these similarities, the driving order parameter of the transitions in LTGO and in LTSO might be, as in

titanite, the off-centre displacement of the transition metal cation. However, the shift of the Ta-cation is not as strictly confined to its bond with the chain-forming O1 oxygen anion as the Ti-shift is in titanite [5]. This probably gives rise to the different behaviour of individual strain components in titanite and in LTSO. Although the order parameter behaves in a very similar way in all three systems, as the diffraction intensities as a function of temperature indicate, the strain coupling to this order parameter differs in titanite and in the two lithiumtantanyl-compounds.

3.3. ^{7}Li MAS NMR

The properties of the isomorphous phase transitions in the two Li-compounds are further examined utilizing the quadrupolar moment of the ^{7}Li nucleus as a probe for the principal EFG component, V_{zz}, and the asymmetry parameter η at the Li-site. As these parameters generally derive from the charge density around a nucleus, they can be accurately obtained by first principle calculation of the electronic structure [23]. In this way structure models can be verified based on the EFG measurements.

As has already been indicated by X-ray structure refinements of LTGO [5], Li occupies a split position in the high-temperature structure of this compound, whereas it orders into one of the two available potential minima below T_c. This picture is confirmed by the ^{7}Li-MAS NMR spectra (Fig. 5). The sideband envelope of the spectrum does not change as a function of temperature up to $T = 290$ K. This indicates that the EFG does not change significantly and hence that the nearest neighbour coordination of Li remains unaltered when crossing the critical temperature. For the disordered phase this signifies that Li oscillates between the two equivalent 8f positions with sufficiently low frequency in order for the position to be resolvable as such by the NMR experiment. The depths of the associated double well potential has been determined as approximately RT_c [5], which suggests that Li oscillates freely between both minima at room temperature.

Electronic structure calculations can be used to obtain information about the theoretical EFG parameters of a given structure type. The atomic positions obtained by force relaxation (Table 1) are in good agreement with the experimental data [3,5], considering the inherent ground state nature of DFT calculations. For the $P2_1/c$ phase simulated spectra based on the computed Li EFG parameters agree well with the observed NMR spectrum. As the spectra hardly change as a function of temperature the calculated parameters match the observed quadrupolar coupling equally well above and below T_c. Fig. 6 demonstrates the discrepancy between simulated and observed spectra if the computed EFG

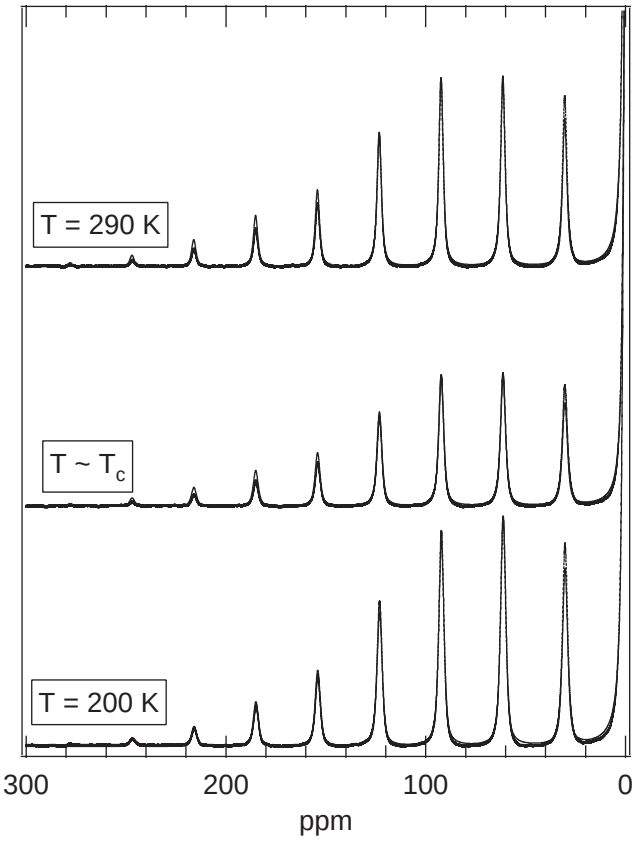

Fig. 5. ^{7}Li MAS NMR spectra (dots) above, below and at the transition temperature of LTGO measured at 194.38 MHz. The curves show the calculated spectra based on the computed quadrupolar coupling parameters ($C_Q = 96$ kHz, $\eta = 0.2$).

parameters of Li in the special 4e position of the $C2/c$ phase are used instead.

A similarly temperature independent sideband envelope is obtained in LTSO. The quadrupolar coupling constant is slightly higher in LTSO, with $\eta \approx 0.5$, as it is equally confirmed by the electronic structure calculations. No significant change of C_Q nor of the asymmetry parameter η is evident from the MAS measurements. However, the static ^{7}Li-spectra of LTSO (Fig. 7) reveal a slight increase of C_Q with rising temperature. In the temperature interval 356–481 K this increase is best described by $C_Q = 76.99 + 0.067$ T. As a similarly small increase would not be detectable in the ^{7}Li-MAS spectra of LTGO, additional static spin echo measurements at 200 K and at 295 K have been carried out using LTGO (L. van Wüllen, personal communication). These spectra indicate an increase of C_Q, namely 86 kHz at 200 K and 95 kHz at 295 K, which is compatible with the temperature increase observed in LTSO.

While the observed increase of the EFG is unusual, it is obvious that the temperature evolution of the EFG is not affected by the structural phase transition. In contrast the dynamic properties of the Li-cation are

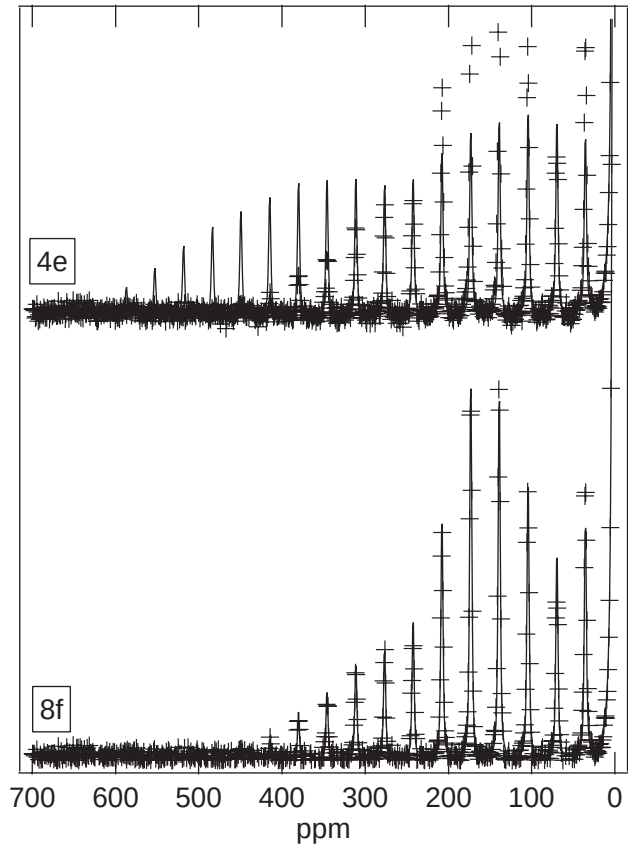

Fig. 6. ^{7}Li MAS NMR spectrum of LTGO at room temperature (crosses) measured at 116 MHz and 4 kHz spinning frequency. The solid curves show the calculated spectra based on the computed quadrupolar coupling parameters for Li occupying either the special 4e position in SG $C2/c$ or the 8f position in SG $P2_1/c$ (cf. Table 2).

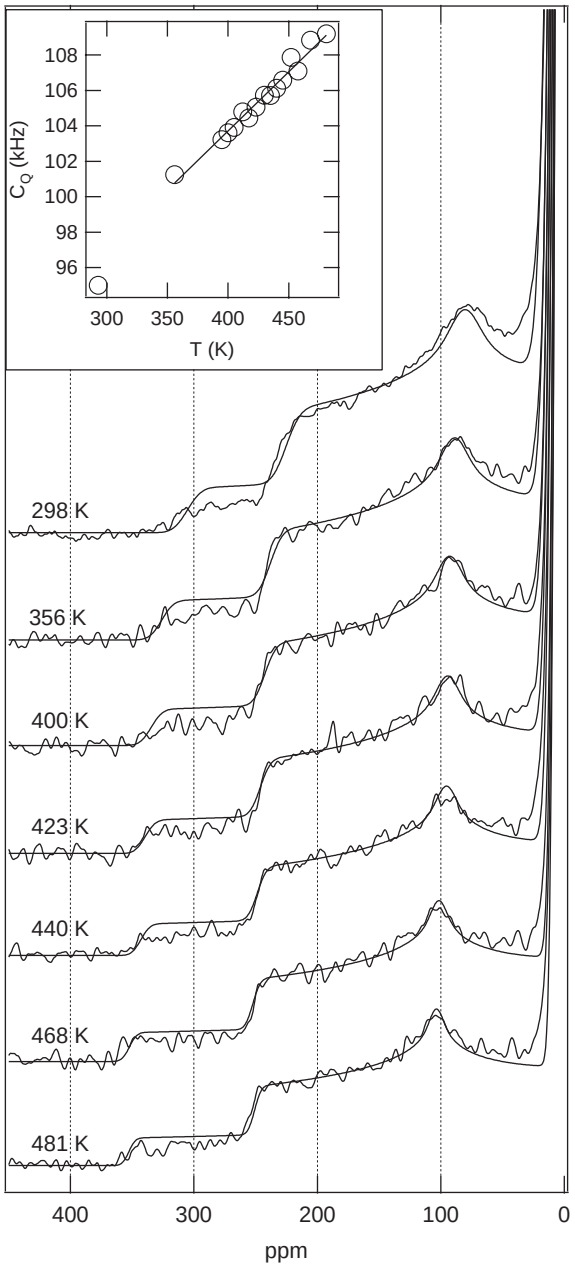

Fig. 7. Measured and simulated static ^{7}Li NMR-spectra of LTSO at selected temperatures. The inset shows the increase of the quadrupolar coupling constant with rising temperature.

influenced by the phase transition. They have visible effect on the NMR spectra as the ^{7}Li–^{7}Li dipole interactions as well as the nuclear quadrupolar couplings are modulated by the atomic motion. Overall enhanced Li mobility is indicated by a significant motional narrowing of the central band with rising temperature in LTSO. Simulation of the dynamic spectra above approximately 400 K is only possible if the sideband envelope and the central transition are modeled using different peak shapes and amplitudes. The resulting temperature dependence of the signal width for the central transition and the spinning sidebands is shown in Fig. 8a. The sidebands remain significantly broader than the central band at high temperatures. The occurrence of the structural phase transition is marked by changes in the shape and width of the bands. Just below the critical temperature of the structural transition the spinning sidebands broaden, while they narrow immediately above it. Such a significant effect on the linewidth is not obvious for the central band. It appears that the inter-site Li-motion within the double well that is associated with the phase transition predominately modulates the satellite transitions. Another effect of the transition on the MAS NMR resonance profiles is the purely Lorentzian profile shape in the vicinity of the transition. As the temperature is lowered the gaussian character decreases approximately linearly, while it increases non-linearly below the transition temperature. This effect is seen both in the sidebands and in the central signal (Fig. 8b). Further work is needed to explore these dynamic aspects of the phase transitions in LTSO and in LTGO by NMR methods.

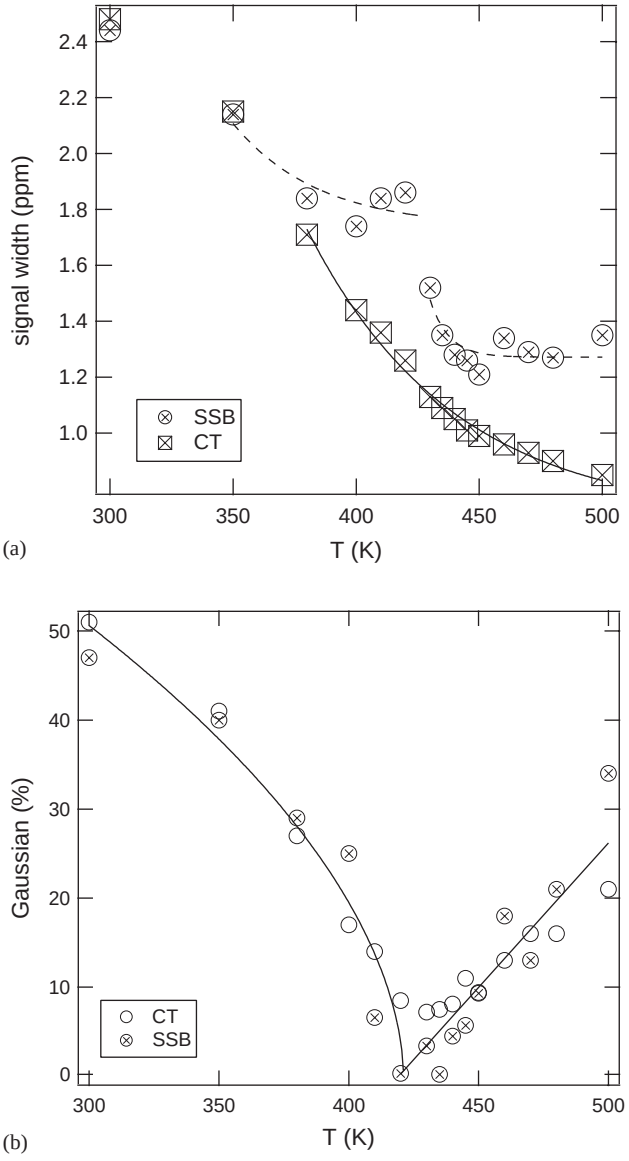

Fig. 8. Motional narrowing in LTSO: (a) Signal width of central peak (CT) and spinning sidebands (SSB) as a function of temperature. The curves are intended to guide the eye. (b) Gaussian component of the peak profiles in percent.

4. Conclusions

^{7}Li MAS NMR does confirm the tetrahedral oxygen coordination of Li both in the high- and low-temperature phases of LTGO and LTSO. In terms of strain and order parameter behaviour the phase transitions in LTGO and LTSO are closely related to the $P2_1/c \leftrightarrow C2/c$ transition in titanite, $CaTiOSiO_4$. The isomorphous substitution of Ge by Si in the two Li-tantanyl compounds causes a large upwards shift of the critical temperature by more than 200 K. The Si–O bond therefore appears to stabilize the displacement of Ta, as realized in the $P2_1/c$-phase.

Acknowledgments

We thank Henning Trill for his help with recording the NMR spectra of LTGO and Hellmuth Eckert for his ongoing support and helpful discussions. The work was funded by *Deutsche Forschungsgemeinschaft*.

References

[1] T. Malcherek, C. Paulmann, M.C. Domeneghetti, U. Bismayer, Diffuse scattering anisotropy and the $P2_1/a \leftrightarrow A2/a$ phase transition in titanite, $CaTiOSiO_4$, J. Appl. Cryst. 34 (2001) 108–113.

[2] M. Taylor, G. Brown, High-temperature structural study of the $P2_1/a \leftrightarrow A2/a$ phase transition in synthetic titanite, $CaTiSiO_5$, Amer. Mineral. 61 (1976) 435–447.

[3] E.A. Genkina, B.V. Mill, Crystal structures of the sphenes $NaSbGeO_5$, $NaTaGeO_5$ and $LiTaSiO_5$, Sov. Phys. Crystallogr. 37 (6) (1992) 769–772.

[4] B. Mill, E. Belokoneva, A. Butashin, Synthesis and crystal structure of compounds $A^{+}M^{5+}GeO_5$ (A = Li, Na; M = Nb, Ta, Sb) and $LiTaSiO_5$, Sov. Phys. Crystallogr. 35 (2) (1990) 176–180.

[5] T. Malcherek, Structure and phase transitions of $LiTaOGeO_4$, Acta Cryst. B 58 (2002) 607–612.

[6] S. Kek, M. Aroyo, U. Bismayer, C. Schmidt, K. Eichhorn, H. Krane, The two-step phase transition of titanite, $CaTiSiO_5$: a synchrotron radiation study, Z. Krist. 212 (1997) 9–19.

[7] M. Zhang, E. Salje, U. Bismayer, Structural phase transition near 825 K in titanite: evidence from infrared spectroscopic observations, Amer. Mineral. 82 (1997) 30–35.

[8] T. Malcherek, Spontaneous strain in synthetic titanite, $CaTiOSiO_4$, Mineral. Mag. 65 (2001) 709–715.

[9] H.K. Cammenga, W. Eysel, W. Gmelin, W. Hemminger, W.G.H. Höhne, S.M. Sarge, Die Temperaturkalibrierung dynamischer Kalorimeter II, Kalibriersubstanzen. PTB-Mitteilungen 102 (1992) 13–18.

[10] H.G. McAdie, P.D. Garn, O. Menis, Standard reference materials: selection of differential scanning analysis temperature standards through a cooperative study, NBS, Special Publication: 260-40, SRM 758, 759, 760, 1972.

[11] D.A. Ditmars, T.B. Douglas, Measurements of the relative enthalpy of pure α-Al_2O_3 (NBS heat capacity and enthalpy reference material No. 720) from 273 to 1173 k, J. Res. NBS A Phys. Ch. 75 (1971) 401–420.

[12] A. Bosenick, C.A. Geiger, L. Cemič, Heat capacity measurements of synthetic pyrope-grossular garnets between 320 and 1000 K by differential scanning calorimetry, Geoch. Cosmoch. Acta 60 (1996) 3215–3227.

[13] S.C. Mraw, Differential scanning calorimetry, in: C.Y. Ho (Ed.), Data Series on Material Properties, Vol. I-2, 1988, pp. 395–437 (Chapter 11).

[14] A. Larson, R. Von Dreele, General structure analysis system (GSAS), Technical Report LAUR B6-748, Los Alamos National Laboratory Report, Los Alamos, New Mexico, 1994.

[15] L.W. Finger, D.E. Cox, A.P. Jephcoat, A correction for powder diffraction peak asymmetry due to axial divergence, J. Appl. Cryst. 27 (1994) 892–900.

[16] D. Massiot, F. Fayon, M. Capron, I. King, S. Le Calvé, B. Alonso, J. Durand, B. Bujoli, Z. Gan, G. Hoatson, Modelling one and two-dimensional solid state NMR spectra, Magn. Reson. Chem. 40 (2002) 70–76.

[17] P. Blaha, K. Schwarz, G.K.H. Madsen, D. Kvasnicka, J. Luitz, WIEN2k, an augmented plane wave + local orbitals program for

calculating crystal properties, Karlheinz Schwarz, Techn. Universitat Wien, Austria, 2001, ISBN 3-9501031-1-2.
[18] J.P. Perdew, S. Burke, M. Ernzerhof, Generalized gradient approximation made simple, Phys. Rev. Lett. 77 (1996) 3865–3868.
[19] S.A. Hayward, J. del Cerro, E.K.H. Salje, Antiferroelectric phase transition in titanite: excess entropy and short range order, Amer. Mineral. 85 (2000) 557–562.
[20] T. Malcherek, C. Paulmann, Diffuse scattering and structural phase transitions of $LiTaOGeO_4$ and $LiTaOSiO_4$, HASYLAB Annual Report, Hamburger Synchrotronstrahlungslabor/DESY, 2002.
[21] M.A. Carpenter, E.K.H. Salje, A. Graeme-Barber, Spontaneous strain as a determinant of thermodynamic properties for phase transitions in minerals, Eur. J. Mineral. 10 (1998) 621–691.
[22] M. Zhang, E. Salje, U. Bismayer, H. Unruh, B. Wruck, C. Schmidt, Phase transition(s) in titanite $CaTiSiO_5$: an infrared spectroscopic, dielectric response and heat capacity study, Phys. Chem. Miner. 22 (1995) 41–49.
[23] M. Iglesias, K. Schwarz, P. Blaha, D. Baldomir, Electronic structure and electric field gradient calculations of Al_2SiO_5 polymorphs, Phys. Chem. Miner. 28 (2001) 67–75.